Engineering with Computers
https://doi.org/10.1007/s00366-022-01659-w

ORIGINAL ARTICLE

Texas TriValve 1.0 : a reverse-engineered, open model of the human tricuspid valve

Mrudang Mathur[1] · William D. Meador[2] · Marcin Malinowski[3,4] · Tomasz Jazwiec[3,5] · Tomasz A. Timek[3] · Manuel K. Rausch[2,6,7]

Received: 8 December 2021 / Accepted: 13 April 2022

Abstract
Nearly 1.6 million Americans suffer from a leaking tricuspid heart valve. To make matters worse, current valve repair options are far from optimal leading to recurrence of leakage in up to 30% of patients. We submit that a critical step toward improving outcomes is to better understand the "forgotten" valve. High-fidelity computer models may help in this endeavour. However, the existing models are limited by averaged or idealized geometries, material properties, and boundary conditions. In our current work, we overcome the limitations of existing models by (reverse) engineering the tricuspid valve from a beating human heart in an organ preservation system. The resulting finite-element model faithfully captures the kinematics and kinetics of the native tricuspid valve as validated against echocardiographic data and others' previous work. To showcase the value of our model, we also use it to simulate disease-induced and repair-induced changes to valve geometry and mechanics. Specifically, we simulate and compare the effectiveness of tricuspid valve repair via surgical annuloplasty and via transcatheter edge-to-edge repair. Importantly, our model is openly available for others to use. Thus, our model will allow us and others to perform virtual experiments on the healthy, diseased, and repaired tricuspid valve to better understand the valve itself and to optimize tricuspid valve repair for better patient outcomes.

Keywords Transcatheter · Repair · Annuloplasty · Predictive simulation · Precision medicine

1 Introduction

Our cardiac valves ensure unidirectional blood flow through the heart and cardiovascular system and, thereby, efficient oxygen transport from the lungs to our body's cells. Consequently, heart valve failure can be devastating to patient health. When heart valves fail, they do so through excessive narrowing that inhibits flow, or through ineffective closure that leads to leakage, i.e., regurgitation. Both modes of failure are associated with significant morbidity and mortality [1–4]. The tricuspid valve, one of our two atrioventricular heart valves, leaks to a significant degree in more than 1.6

✉ Manuel K. Rausch
manuel.rausch@utexas.edu

Mrudang Mathur
mrudangm@utexas.edu

William D. Meador
william.meador@utexas.edu

Marcin Malinowski
mmalinowski@icloud.com

Tomasz Jazwiec
thomas.jazwiec@gmail.com

Tomasz A. Timek
tomasz.timek@spectrumhealth.org

[1] Department of Mechanical Engineering, University of Texas at Austin, Austin, TX 78712, USA

[2] Department of Biomedical Engineering, University of Texas at Austin, Austin, TX 78712, USA

[3] Cardiothoracic Surgery, Spectrum Health, Grand Rapids, MI 49503, USA

[4] Department of Cardiac Surgery, Medical University of Silesia School of Medicine in Katowice, Katowice, Poland

[5] Department of Cardiac, Vascular and Endovascular Surgery and Transplantology, Medical University of Silesia in Katowice, Silesian Centre for Heart Diseases, Zabrze, Poland

[6] Department of Aerospace Engineering & Engineering Mechanics, University of Texas at Austin, Austin, TX 78712, USA

[7] Oden Institute for Computational Engineering and Sciences, University of Texas at Austin, Austin, TX 78712, USA

Published online: 24 May 2022

million Americans [5]. In most of those patients, the tricuspid valve leaks because its normal shape and dynamics have been disrupted by a dilated and remodeled right ventricle, to which it is intimately connected through its annulus and chordae tendineae. Causes for right-ventricular remodeling include pulmonary hypertension for example [6, 7]. Unfortunately, in the patients that are treated for tricuspid valve regurgitation, surgery has a significant failure rate. In fact, 10–30% of patients present with recurring regurgitation within a few years of surgery [8–10]. Because the tricuspid valve has long been ignored—earning it the nickname "the forgotten valve" [11, 12]—we submit that an incomplete understanding of the tricuspid valve is, at least in part, responsible for these high failure rates.

Computational models of the tricuspid valve could be useful tools in our effort to better understand the valve [13]. Specifically, high-fidelity computer models of the tricuspid valve may support studies on the etiological reasons for the valve's shape, structure, and dynamics, which, to date, are mostly unknown. Additionally, computer models may allow us to mechanistically understand suboptimal clinical outcomes and serve to optimize medical devices [14, 15]. Notably, most of today's models are based on idealized or population-averaged geometries; see Table 1. However, in reality, no heart valve is identical to another one, and ignoring significant between-subject variability may impede progress on understanding tricuspid valve disease and improving repair techniques and outcomes. Similarly, mechanical and structural properties are often assumed or derived from other subjects or, yet, other species. Additionally, most previous models have not been made openly available as an accessible tool (see references in Table 1).

The objective of this current work is therefore twofold. First, our goal is to build a subject-specific, high-fidelity finite element model of the human tricuspid valve and to demonstrate potential applications of our model. Secondly, our goal is to make our model openly available to the scientific and medical community.

2 Methods

We established a complete (reverse) engineering pipeline to reconstruct a highly detailed finite-element model of the healthy human tricuspid valve; see Fig. 1. To this end, we loaded the right heart of a healthy, beating human heart within an organ preservation system to recreate a realistic hemodynamic environment for the valve. Within the organ preservation system, we measured tricuspid annulus dynamics via fiducial markers and collected hemodynamic data via miniaturized pressure sensors in the right atrium and ventricle throughout the cardiac cycle. Upon conclusion of the ex vivo experiments, we excised the tricuspid valve and characterized its geometry and mechanical properties. To build the model geometry, we then combined the fiducial-marker-based reconstructions of the tricuspid annulus with image-based planimetry of the valve leaflets. Through in vitro images, we also identified chordal insertion sites and included them in our model definition. Additionally, we imposed subject-specific Neumann and Dirichlet boundary conditions as transvalvular pressure gradients (measured via miniaturized pressure sensors) and annular dynamics (measured via epicardial echocardiography and fiducial-marker measurements), respectively. Finally, we assigned subject-specific hyperelastic material properties to all three leaflets and their chordae tendineae based on planar biaxial mechanical tests and uniaxial tensile tests, respectively, on the excised tissue. Detailed descriptions of the reverse engineering pipeline are provided below.

Table 1 Comparison of our current model to existing computational models of the tricuspid valve

	Species	Geometry	Material Properties	Dirichlet B.C.	Neumann B.C.	Openly Available
Stevanella et al. [16]	Porcine	Generic	Generic	N/A	Generic	No
Kong et al. [17]	Human	Specific	Generic	Specific	Generic	No
Kamensky et al. [18]	Porcine	Generic	Generic	N/A	Generic	No
Laurence et al. [19]	Porcine	Specific	Generic	N/A	Generic	No
Singh-Gryzbon et al. [20]	Porcine	Specific	Generic	N/A	Generic	No
Laurence et al. [21]	Generic	Generic	Generic	N/A	Generic	Yes
This work	**Human**	**Specific**	**Specific**	**Specific**	**Specific**	**Yes**

The bold values highlight and compare features of the present work against existing literature

B.C. boundary condition

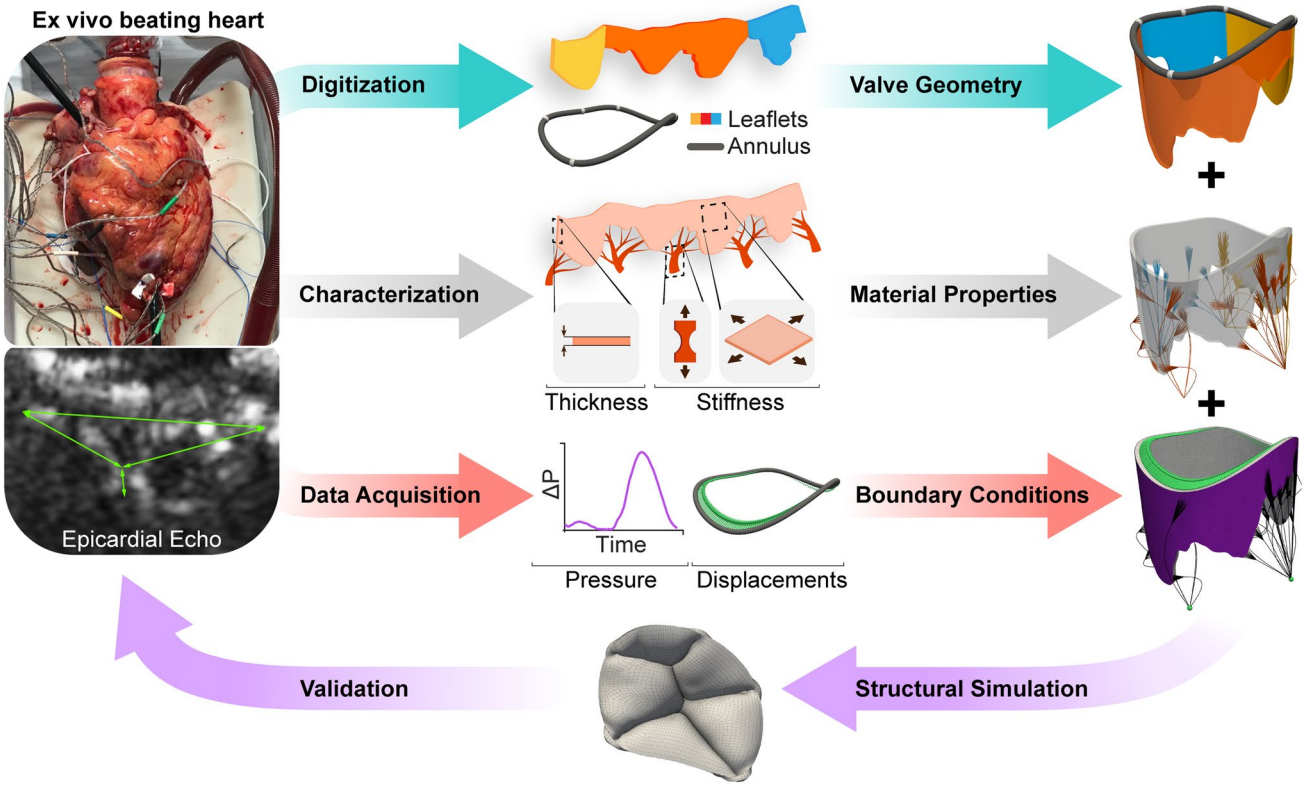

Fig. 1 The (reverse) engineering pipeline. We built a high-fidelity finite-element model of the tricuspid valve from ex vivo and in vitro measurements on a healthy, beating human heart. That is, we built the model geometry by digitizing the valve annulus from fiducial marker measurements on the beating heart and by digitizing the leaflet geometry from photos of the explanted leaflets. We also identified the material properties for our model based on in vitro mechanical tests of each leaflet and their chordae tendineae. The pressure boundary conditions on the leaflet surface and the displacement boundary conditions on the dynamically contracting annulus were also acquired in the beating heart. Finally, we used the explicit finite-element method to predict valve closure which we then validated against beating heart epicardial echocardiographic images

2.1 Beating heart preparations and measurements

The use of rejected human donor hearts was declared nonhuman research by the Spectrum Health Institutional Review Board.

The human donor heart we used in this study was rejected from clinical transplantation but found to be structurally healthy. Please see our previous publication for surgical details of the explantation protocol [22]. During transport from the donor site, the heart was protected with cold HTK-Custodial solution (Essential Pharmaceuticals, Durham, NC). Upon receipt, we implanted six sonomicrometry crystals (Sonometrics Inc., London, Ontario, Canada) in the arrested heart around the tricuspid annulus and three crystals on the papillary muscle heads via a right atriotomy [23]. Additionally, we placed pressure transducers (PA4.5-X6; Konigsberg Instruments Inc., Pasadena, CA) in the right ventricle and the right atrium. Following the instrumentation of the heart, it was prepared for connection to an organ preservation system (TransMedics, Andover, MA). This portable ex vivo organ perfusion platform is being used clinically to perfuse beating, unloaded donor hearts with warm, oxygenated blood during transport between donation site and transplant site. In our study, we primed the system with donor blood, mounted the instrumentalized heart, and defibrillated the heart to return to normal sinus rhythm. Subsequently, we paced the heart at 80 beats per minute and continued perfusing it under normoxic conditions. During data collection, we collected arterial and coronary sinus venous blood gases, including lactate levels every 15 min to assure stability of the experimental preparation. After 60 min of reperfusion, we partially occluded the pulmonary artery to increase right ventricular pressure to approximately 30 mmHg to simulate loaded conditions. At this point, we assessed tricuspid valve competence via epicardial echocardiography (Vivid S6, GE Healthcare, Chicago, IL). Once we established complete valve competence, we recorded hemodynamic data and sonomicrometry data under working right-heart conditions.

2.2 Tricuspid valve collection and tissue preservation

After all measurements on the beating heart were concluded, we arrested the heart and surgically removed the tricuspid valve. Upon excision, we cut the valve annulus at the posterior-septal commissure and laid the valve complex (including chordae tendineae) on a calibrated grid on which we took detailed photographs. Subsequently, we isolated each leaflet and froze them at – 80°C in a cryogenic solution of 9:1 DMEM and DMSO with protease inhibitor (Pierce, Thermo Scientific, Waltham, MA) via a controlled freezing device (Mr. Frosty, Thermo Scientific, Waltham, MA, USA)[24].

2.3 Mechanical testing

Before mechanical testing, we thawed the frozen tissue samples in room-temperature phosphate-buffered saline. Once thawed, we separated the chordae tendineae from the leaflets. For mechanical characterization of the leaflet tissue, we excised 7×7 mm tissue samples from the leaflet centers, measured the sample thickness in three regions with a digital thickness gauge (547-500S, Mitutoyo Corp., Kawasaki, Japan), marked fiducial dots for strain tracking with black markers, and mounted the samples to our planar biaxial tensile tester (BioTester, Cellscale, Waterloo, ON, Canada). Once mounted, we conducted force-controlled 400 mN equibiaxial mechanical tests, using methods described in detail by Meador et al. [25]. Additionally, we excised three chordae tendineae from each leaflet and measured their thickness at three points along their length under a 4× objective on an optical microscope (BX53 Upright Microscope, Olympus Life Science, Waltham, MA). To quantify the constitutive behavior of the chordae tendineae, we mounted them to our uniaxial tensile testing device (Univert, Cellscale, Waterloo, ON, Canada) and performed force-controlled uniaxial tensile tests as described in detail in our previous work [26].

2.4 Constitutive modeling

We modeled the tricuspid valve leaflets as a hyperelastic material. To this end, we cast their constitutive behavior into the form of a two-term strain energy function, viz.

$$W(\mathbf{C}) = \frac{c_0}{2}\left[I_1 - 3\right] + \frac{c_1}{2}\left[\exp(c_2[I_1 - 3]) - 1\right], \tag{1}$$

where $I_1 = \mathbf{C} : \mathbf{I}$ with $\mathbf{C}$ being the right Cauchy–Green deformation tensor and $\mathbf{I}$ being the second-order identity tensor. In the above expression, the first term determines the tissue response at small strains and under compression, while the second term dictates the strain-stiffening response of the tissue at large positive strains. This model was suggested by Kamensky et al. [18] and reflects our previous work on the detailed characterization of the ovine tricuspid valve leaflets [27]. Note, while the valve leaflets are generally described as anisotropic, their degree of anisotropy is minimal [28]. During preliminary studies, we found equivalently good fits for the above isotropic model as for similar, anisotropic forms. We thus chose the above relation as it requires fewer parameters and was significantly more stable.

Similarly, we modeled the chordae tendineae as hyperelastic materials. Our previous work [26] has shown excellent fits via the Ogden model, viz.

$$W\left(\lambda_1, \lambda_2, \lambda_3\right) = \sum_{i=1}^{3} \frac{2\mu_i}{{\alpha_i}^2}\left[{\lambda_1}^{\alpha_i} + {\lambda_2}^{\alpha_i} + {\lambda_3}^{\alpha_i} - 3\right], \tag{2}$$

where $\lambda_{1/2/3}$ are the principal stretches.

We fit the constitutive parameters for the leaflet models and the chordae tendineae models using a least-squares approach as implemented in MATLAB 2020a (Mathworks, Natick, MA). Specifically, we fit the parameters by minimizing the error between our experimental measurements and analytical solutions to the planar biaxial and uniaxial boundary value problem for which we assumed that the materials behaved incompressibly. For the leaflets, we fit models to data from one equibiaxial test mode per leaflet. For the chordae tendineae, we simultaneously fit the uniaxial data of three chordae tendineae samples from each leaflet. Detailed descriptions of model fits for this study are provided in Supplementary Figs. S1, S2 and Tables S1, S2.

2.5 Geometry digitization and discretization

We followed a multi-step process to combine ex vivo and in vitro measurements to create a digital representation of the tricuspid valve; see Fig. 2. Based on the sonomicrometry data that we collected in the beating human hearts, we first triangulated the positions of six fiducial-marker points along the tricuspid annulus: one at each commissure and one at the midpoint between each commissure. Subsequently, we used a least-squares algorithm to identify a cubic spline that optimally fit these points (Fig. 2a) and parameterized the arc length of this spatial curve, similar to previous studies [29–32].

Next, we identified the leaflet geometry from photos of the full valve apparatus. To this end, we first corrected image distortions caused by a non-orthogonal camera perspective in Photoshop CC 2019 (Adobe Inc., San Jose, CA) before we outlined the valve annulus and valve free edge via splines using a custom MATLAB script (Fig. 2b). Next, we parameterized the leaflet height, i.e., distance between annulus and free edge, as a function of annular location.

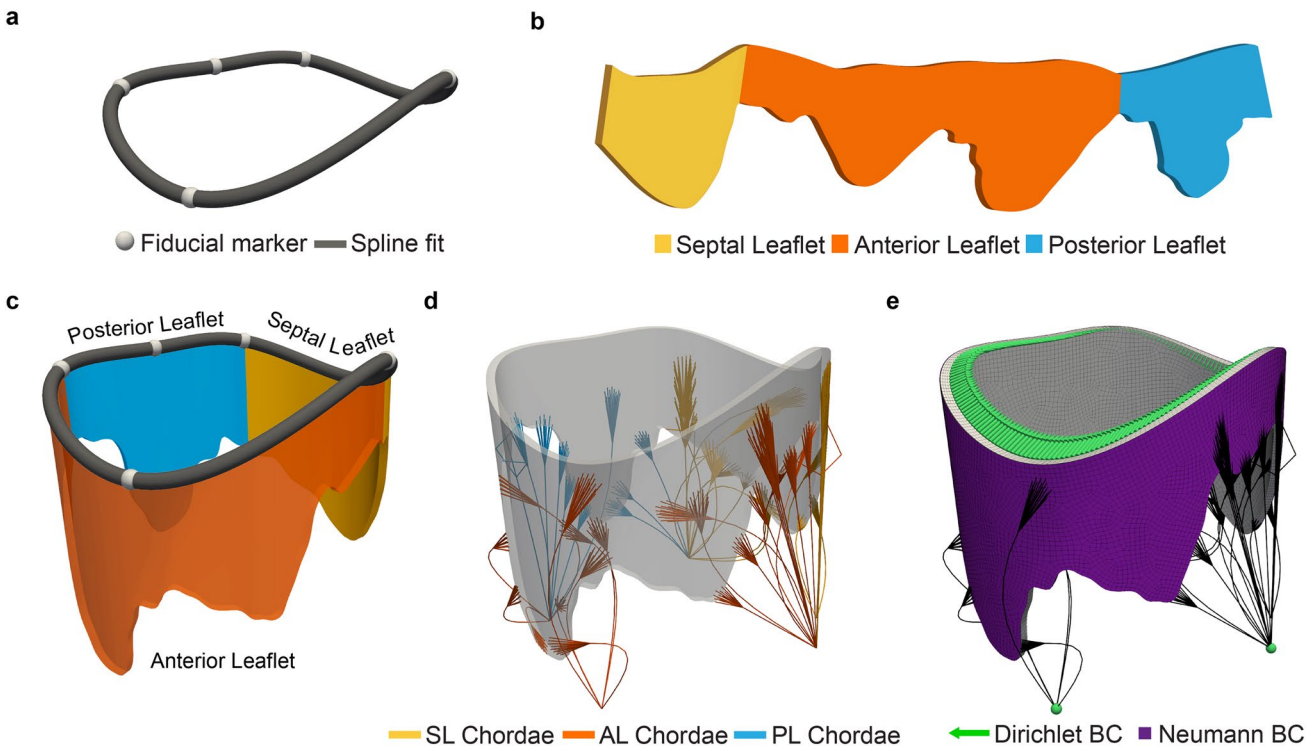

Fig. 2 In silico model reconstruction pipeline. **a** We fit a periodic cubic spline to fiducial-marker positions to create a three-dimensional representation of the tricuspid annulus. **b** Next, we digitized the leaflet geometry from valve images, and **c** non-rigidly transformed the leaflet geometry onto the annulus to obtain a stress-free reconstruction of the valve. **d** Chordal insertions were subsequently created for each leaflet. **e** Finally, we assigned subject-specific annular displacement and transvalvular pressure gradients, i.e., Dirichlet and Neumann boundary conditions, respectively, to the model

To assemble the full 3D representation of the tricuspid valve, we vertically projected the photogrammetry-based leaflet heights from the sonomicrometry-based annulus. Next, we imported both spatial curves into the meshing software Cubit 2020.2 (Coreform LLC, Orem, UT), where we fit spline surfaces between these curves [33]. Next, we applied an averaged leaflet thickness to the resulting surfaces to create subject-specific valve volumes (Fig. 2c). Also, in Cubit, we meshed these surfaces with hexahedral elements. Finally, we identified chordal insertion points on each leaflet based on photographs and literature data [34]. Similarly, we identified spatial coordinates of papillary muscle heads based on sonomicrometry data and literature data. We used multiple one-dimensional structural elements to connect each leaflet insertion point and the papillary muscle head coordinates (Fig. 2d) [35, 36]. To avoid stress singularities, we spatially distributed chordal insertions near the leaflet [37, 38], see Supplementary Fig. S6. Further details on solver specific element choices are provided below.

2.6 Boundary conditions

We modeled the valve under both quasi-static and dynamic loading conditions. Under quasi-static loading, we simulated the valve from end-diastole to end-systole. To account for annular contraction, we first computed the annular configuration for each simulation timepoint based on our sonomicrometry data. Between those timepoints, we then computed the displacement vector for every leaflet mesh point on the annular leaflet boundary (Fig. 2e). Additionally, we applied an end-systolic, transvalvular pressure of 22.95 mmHg (as measured ex vivo) to the ventricular surface of our valve. Similarly, in our dynamic simulations, we applied annular displacements and transvalvular pressures as measured at each timepoint during one cardiac cycle. In all simulations, we simultaneously applied both displacements and pressure gradients in a single simulation step.

2.7 Chordal length adjustments

While chordal constitutive properties, diameters, and insertion and origin sites were informed from subject measurements, we did not know the exact, in vivo length of each chord. To identify those lengths, we performed a manual optimization. That is, we followed a similar strategy as outlined by Kong et al. [39]. Specifically, we modeled the

chordae tendineae as sinusoidal segments. Thus, by altering each segment's amplitude in the end-diastolic state, we could adjust its length without having to alter the papillary muscle head coordinate or the insertion site. Subsequently, we successively lengthened or shortened each chord until we achieved optimal valve closure, which we defined as that closure that provided a continuous seal among all leaflets and aligned the free edges of opposing leaflets.

2.8 Numerical simulations

We conducted all simulations in Abaqus/Explicit 6.20-1 (Dassault Systémes, Vélizy-Villacoublay, France). To this end, we imported the discretized valve in Abaqus and applied boundary conditions as described above. We chose the chordae mesh density based on similar work by Pham et al. [40] and chose leaflet in-plane mesh density as well as mesh layer number according to careful sensitivity studies and in direct consultation with the Abaqus Living Heart Team [41]; see Supplementary Fig. S3. For the leaflet volume elements, we chose the reduced integration hexahedral C3D8R elements, while we chose the truss element T3D2 for the chordae tendineae. Based on in vitro measurements of the valve, we assigned a uniform thickness of 0.78 mm to the valve leaflets and a diameter of 0.65 mm to anterior, 0.64 mm to posterior, and 0.71 mm to septal leaflet chordae tendineae in our model.

In all simulations, we modeled the leaflets as nearly incompressible solids and enforced this constraint by penalizing volumetric deformations via a bulk modulus that resulted in a Poisson's ratio of 0.495 (i.e., 99.67 kPa). Note, we implemented these constraints through the Abaqus subroutine *VUANISOHYPER_INV* [42]. Additionally, we modeled contact between leaflets using Abaqus' kinematic contact constraint [43], but did not model contact between chordae tendineae and leaflets. Furthermore, we employed uniform mass scaling to maintain a minimum time step of $\Delta t = 1 \times 10^{-6}$ s and $\Delta t = 1 \times 10^{-7}$ s in our quasi-static simulations of the healthy and diseased valve, respectively. In our dynamic simulations, we used a stable time step determined by Abaqus/Explicit.

2.9 Pathological valve model

To determine the effects of disease- and repair-induced changes to tricuspid valve mechanics, we modified our predictive model to resemble the tricuspid valve as seen in patients with pulmonary arterial hypertension-induced functional tricuspid regurgitation. To this end, we asymmetrically dilated the tricuspid annulus [44] and free edge, induced leaflet tethering by apically displacing the papillary muscles [45], and applied an elevated transvalvular pressure load of 42.5 mmHg to our model [46]. Further details on creating the pathological valve are provided in Supplementary Fig. S4. Next, we virtually repaired the valve through ring-based annuloplasty and clip-based edge-to-edge repair techniques. Specifically, we implanted a size 30 Carpentier-Edwards Physio Tricuspid Annuloplasty Ring (Edwards Lifesciences, Irvine, CA), which we digitized in a previous study [47]. Furthermore, we performed edge-to-edge repair using two MitraClip devices (Abbott Laboratories, Chicago, IL) placed between the anterior and septal leaflets. Here, we built a simplified version of the clip arms using device dimensions provided by Lesevic et al. [48].

2.10 Annuloplasty simulations

To virtually repair the diseased valve via ring-based annuloplasty we first pretensioned the chordae tendineae as previously described [40]. Next, we aligned the midline of the annuloplasty ring with the valve annulus. Specifically, we fixed one end of the ring at the anteroseptal commissure and rotated the ring into place while ensuring that the general region around the atrioventricular node was uncovered by the ring. Next, we displaced every third node along the covered annulus to match a corresponding location on the annuloplasty ring, thereby mimicking annular approximation via sutures, similar to Kong et al. [17]. We emulated the anchoring effect of the intraventricular septum by limiting the motion of the uncinched septal annulus with a Link-type multi-point constraint in Abaqus. Here, the relative distance between each of the constrained nodes is held constant during the simulation. Finally, we applied pathological pressure loads to the ventricular surface of the valve.

2.11 Clip-based repair simulations

To perform a simplified edge-to-edge repair on the regurgitant valve, we followed the strategy detailed in a similar analysis performed on the mitral valve [49]. Briefly, we first digitized a model of the MitraClip device and discretized it as a rigid body with R3D4 elements in Abaqus. We then assigned a rough contact constraint on the inner surface of the MitraClip arms where the device interacts with the leaflets and placed the two arms at a distance of 1.4 mm from one another [50]. Next, we implanted two MitraClip devices in the regurgitant tricuspid valve at the end-systolic state. We then removed the pressure load on the ventricular surface of the leaflets to allow them to fall onto the clip arms before the clips were closed. Finally, we re-applied pathological pressures quasi-statically to the leaflet surfaces and simulated the end-systolic state of the repaired valve. It is important to note that we pinned the valve annulus during this process.

2.12 Augmented reality visualizations

To enhance the spatial visualization of our finite-element results, we built Augmented Reality (AR) models of the tricuspid valve in the end-systolic state. Specifically, we exported our simulations results from ParaView 5.6 (Kitware Inc., Clifton Park, NY) to Blender 2.9 (Blender Institute B.V, Amsterdam, Netherlands) where we created AR models compatible with Android and iOS devices. The AR models created are openly accessible at the GitHub repository associated with this article; see Data Availability.

3 Results

3.1 Model validation against epicardial echocardiography in the beating heart

For validation of our model, we imposed the subject-specific end-systolic Neumann and Dirichlet boundary conditions and quasi-statically simulated full closure of the valve with the explicit finite-element method. We then compared the 3D valve geometry to the 2D echocardiographic data collected in the beating human heart. To this end, we first identified the echocardiographic imaging plane in our 3D model; see Fig. 3, Supplementary Video 1, and AR Model 1. Next, we measured distances between key landmarks in both the echocardiographic images and in our 2D cut-plane of the 3D model. Specifically, we identify four landmarks: anterior leaflet hinge point (A), septal leaflet hinge point (S), point of coaptation between the two leaflets (C), and the coaptation point of the leaflet free edges (T). Based on these measurements, we found that our model configuration closely matched our echocardiographic data: We found an S–A distance of 22.9 mm in both model and experiment, an S–C distance of 10.6 mm and 10.7 mm in model and experiment, respectively, an A–C distance of 13.6 mm and 14.0 mm again in model and experiment, respectively, and a C–T distance of 4.4 mm and 2.8 mm in the model and experiment, respectively. The small variations between model and experiments fall well within the expected error of 1.4–3 mm in 2D echocardiographic measurements [51]. See also Fig. 4a, b and AR Model 2 for a depiction of leaflet stress and stretch in the quasi-statically loaded valve.

3.2 Dynamic model predictions over the cardiac cycle

After validating the predicted leaflet configuration at end-systole against our echocardiographic measurements in the beating heart, we next investigated the predicted dynamic behavior of our valve. To simulate the dynamics of the tricuspid valve over the cardiac cycle, we applied transient annular displacement and transvalvular pressure gradient boundary conditions as measured ex vivo to our valve model; see Fig. 4c and Supplementary Video 2. Note that the timepoints t_1 through t_8 are depicted in

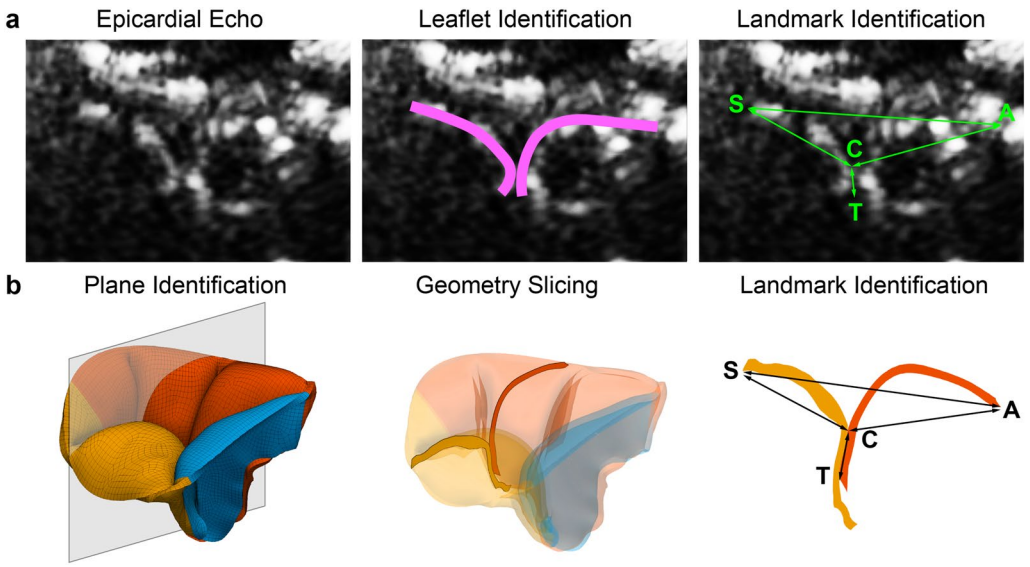

Fig. 3 Model validation against beating heart echocardiography. **a** To validate our valve simulations, we first measured the distances between the anterior (A) and septal (S) leaflet hinge points as well the coaptation point (C) and coaptation length (T) in 2D echocardiographic images in the beating heart. **b** We then identified the corresponding imaging plane in our finite-element model and repeated the same measurements as in the echocardiographic images for comparison. Note that, in the above echocardiographic images, we increased contrast and saturation values to improve leaflet visibility

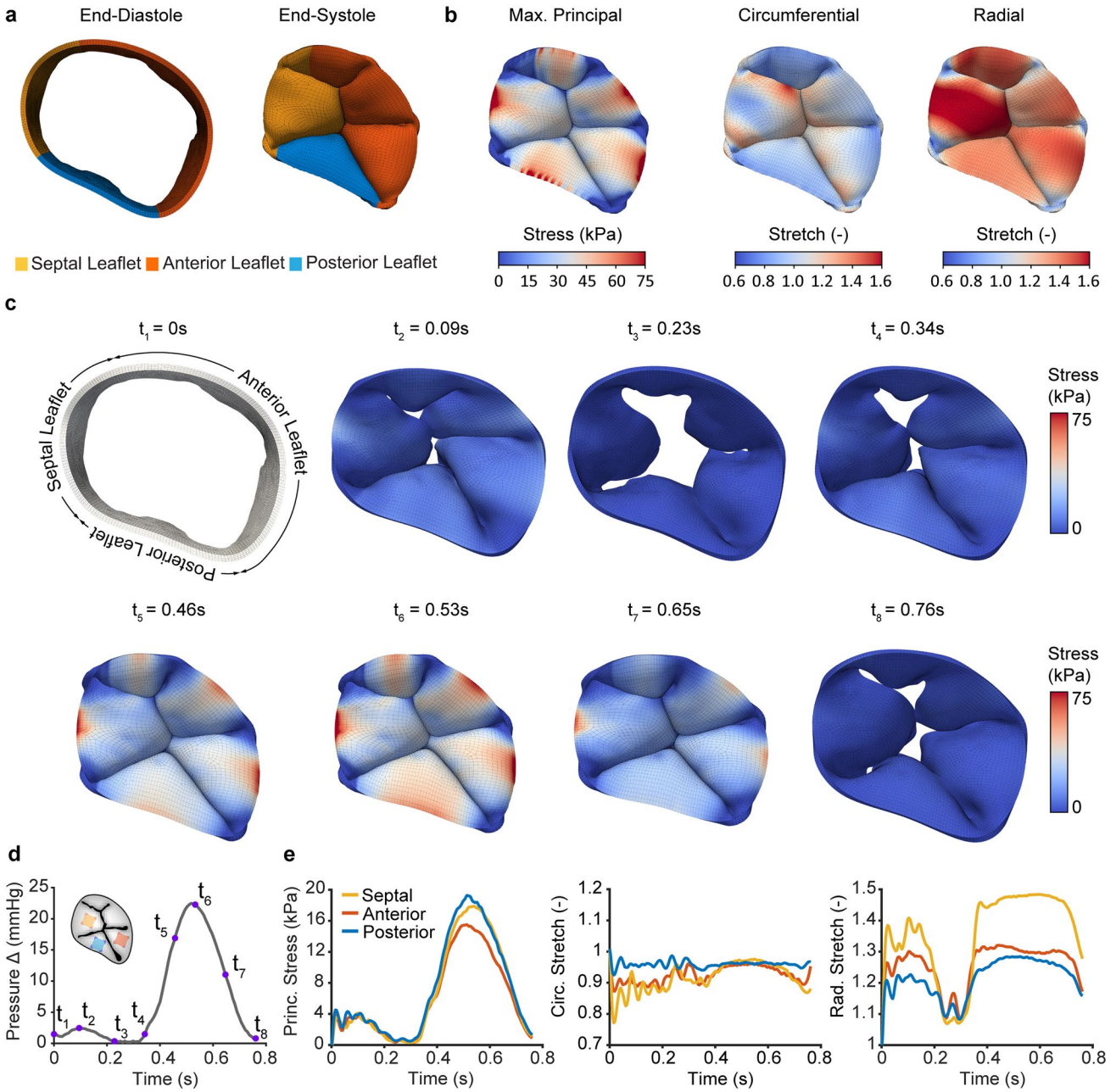

Fig. 4 Predicted kinematics and kinetics of the tricuspid valve model. **a** Quasi-static, tricuspid valve coaptation between end-diastolic and end-systolic states. **b** Measures of quasi-static principal stress as well as radial and circumferential leaflet stretch at end-systole. **c** Dynamic tricuspid valve closure at seven timepoints over the cardiac cycle where we show maximum principal Cauchy stress as a measure of the valve's mechanics. **d** Transient pressure gradient applied to the ventricular surface of the valve. Inset: leaflet centers. **e** Evolution of critical measures of valve mechanics as averaged over the leaflet centers depicted in (**d**)

Fig. 4d. As a measure of valve mechanics, we show the maximum principal Cauchy stress that shows notable heterogeneity across the valve with larger stresses near the annular boundary and the leaflet bellies. Conversely, the model predicts small or negative stresses near the commissures where bending dominates the mechanics of the valve leaflets. These findings match those of others both qualitative as well as quantitatively [19, 20, 39], see Supplementary Fig. S5 for a direct, quantitative comparison of leaflet stresses in our and others' findings. To further visualize the temporal evolutions of leaflet mechanics, Fig. 4e shows the maximum principal Cauchy stress as well as radial and circumferential stretches throughout the cardiac cycle.

These data reflect our own and other previous reports on leaflet mechanics in that leaflets show significant stress heterogeneity (as also shown in the full field results in Fig. 4c) and strong anisotropy with stretches being much greater in the radial direction than the circumferential direction [39, 52].

3.3 Virtual case studies

After validating our model and demonstrating its ability to faithfully capture the kinematics and kinetics of the healthy tricuspid valve, we also demonstrate its usefulness in two virtual case studies. To this end, we modified our model to create a diseased tricuspid valve; see Supplementary Fig. S4 and AR Model 3. That is, we altered model geometry and boundary conditions to induce functional tricuspid valve regurgitation. Then, we virtually repaired the diseased valve with two alternative repair strategies. First, we implanted a commercially available annuloplasty ring in our diseased valve; see Fig. 5, Supplementary Video 3, and AR Model 4 for the simulated implantation procedure. Second, we also simulated repair via transcatheter-based edge-to-edge repair with two clips; see Fig. 6, Supplementary Video 4, and AR Model 5.

Figure 7a shows the healthy valve, the diseased valve, the valve repaired via annuloplasty, and the valve repaired via clips at end-systole. The diseased valve clearly shows a dilated annulus and the arising gap in the coaptation line, i.e., the regurgitant orifices. Additionally, it shows that disease-induced dilation and hypertension led to significant increases in leaflet stresses near the annulus. After repair via annuloplasty, the valve shows a clear reduction in size, but also suture-induced stress risers and an overall leaflet configuration that differs from the original valve. Moreover, after clip-based repair, the regurgitant orifices are gone, but the valve has not significantly changed in size or in stress

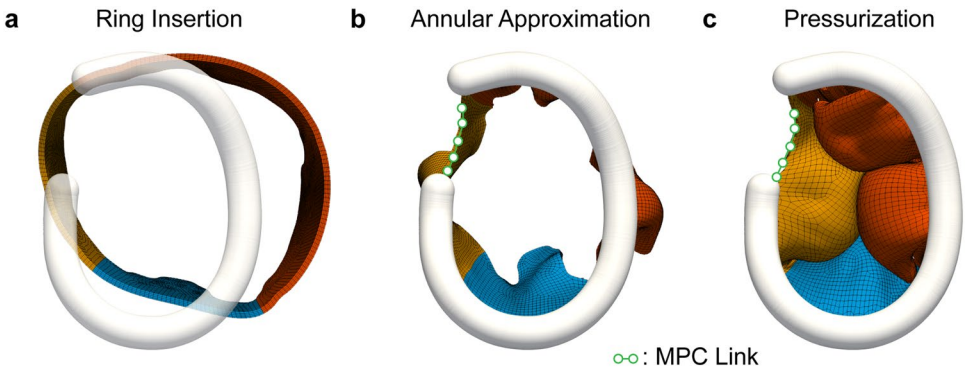

Fig. 5 Showcase 1: Simulated (surgical) implantation of a tricuspid valve annuloplasty device. **a** The annuloplasty ring is first aligned with the tricuspid annulus. **b** Displacements are applied to the model annulus to match the ring geometry, while open-segment motion is modeled via multi-point constraints (MPC). **c** The valve is pressurized

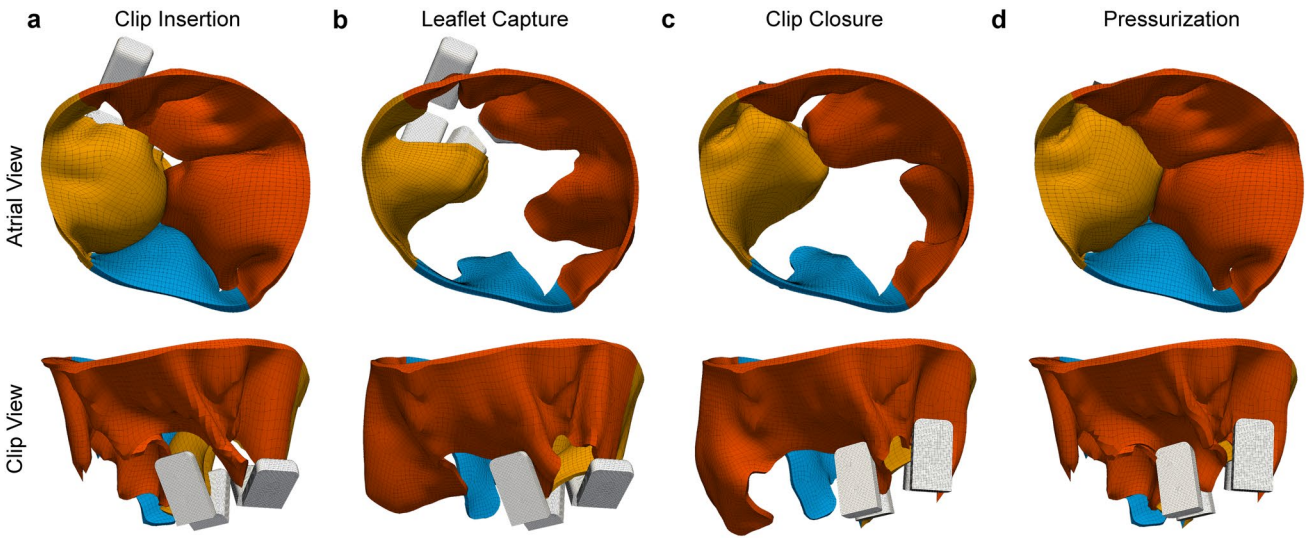

Fig. 6 Showcase 2: Simulated (transcatheter) implantation of tricuspid valve clips. **a** Two clips are inserted in gaps between the anterior and septal leaflets, while the valve is in the closed, pressurized configuration. **b** Pressure loads are removed to allow the clips to capture leaflets. **c** The clips are closed. **d** The valve is pressurized

Table 2 Area measures of the healthy, diseased, and repaired tricuspid valve models at end-systole

Area (mm^2)	Healthy	Diseased	Annuloplasty	Clip-based repair
Orifice	400	870	534	870
Leaflet	1356	2236	2051	2258
Coaptation	577	228	607	265

Table 3 Leaflet stresses of the healthy, diseased, and repaired tricuspid valve at end-systole. Maximum principal Cauchy stress values are calculated in the center of each leaflet

Leaflet stress (kPa)	Healthy	Diseased	Annuloplasty	Clip-based repair
Anterior	16.82	83.61	38.07	84.27
Posterior	15.12	63.65	35.43	66.44
Septal	21.90	87.97	57.75	99.14

distributions from the diseased valve. Figure 7b further illustrates the impact of repair on valve coaptation. That is, we identified the surface elements of the finite-element valve models that actively engaged in coaptation via their contact pressure [53]. The figure clearly shows that the overall contact, i.e., coaptation, area is reduced in the diseased valve but mostly restored after annuloplasty. While the clip-based technique may have diminished any regurgitant orifices, it failed to restore the healthy coaptation competence. Table 2 summarizes the results of our simulations quantitatively by comparing orifice area, leaflet area, and coaptation area between the healthy, diseased, and repaired valves. Similarly, Table 3 summarizes the results of our simulations quantitatively by comparing maximum principal Cauchy stress in the leaflet centers between healthy, diseased, and repaired valves. Together, the data in Tables 2 and 3 reflect the findings in Fig. 7: While annuloplasty mostly recovers pre-disease coaptation area, clip-based repair does not. Additionally, because of the altered loading of the diseased valve, neither repair technique recovers pre-disease valve stresses.

4 Discussion

Detailed computer models of the tricuspid valve may help to improve the currently poor clinical outcomes associated with tricuspid valve repair [54]. To overcome the current gap in highly detailed, subject-specific finite-element models of the human tricuspid valve, we presented such a model in our current work. That is, we presented a high-fidelity model of the human tricuspid valve that is informed by subject-specific geometries, material properties, and boundary conditions. We validated our model against echocardiographic images of the tricuspid valve in a beating human heart. Subsequently, we examined the predicted kinematics and kinetics of the simulated valve throughout the cardiac cycle, and found that it faithfully captures our own and others' findings in animals and humans with the exception of small deviations. That is, we observed some difference in leaflet strains between our current study and previous in vivo experiments [52]. Specifically, we observed the largest strains in the septal leaflet in our model, while we observed the largest strains in the anterior leaflet in our experiments. We attribute these differences to inter-subject variability of the tricuspid valve and potential inter-species variability between humans and sheep. Next, we showcased our model by creating a diseased valve model and then virtually repairing this diseased valve using both a surgical technique and a transcatheter approach. Thus, we fulfilled our primary objective of building and validating a subject-specific, high-fidelity finite-element model of the human tricuspid valve and of demonstrating its usefulness in two showcases.

Importantly, our objective was twofold. In addition to our primary objective, we also aimed at providing this tool openly to the wider scientific community. Our motivation to make our data available was largely driven by the uniqueness of our data set and the unlikeliness for similar, future endeavours. That is, our ability to collect data on healthy, beating, human hearts was the result of multiple fortuitous factors that will be difficult to recreate by others. For example, we benefited from the simultaneous availability of the organ preservation system, the availability of non-transplanted healthy human hearts, the availability of the sonomicrometry technology, the availability of the transplant surgery team, and the availability of the dedicated research staff. To maximize the impact of our data and make our model openly available, one critical choice was that of which finite-element software to use; we chose Abaqus/Explicit. While this choice may at first be counterintuitive for an open science project—given the commercial nature of the software—our reasons were as follows. Our model requires two types of numerical elements: continuum elements to model the leaflets, and 1D truss elements to model the chordae tendineae. Open-source software packages such as FEBio or FEniCS currently have no standard implementations of 1D truss elements. While both packages, and most others, allow for user implementations of truss elements through plug-ins and similar mechanisms, such modifications often require advanced mechanics and programming skills that the wider scientific (and especially medical) community may not have [55]. Additionally, while Abaqus is a commercial software package, many institutions have access to Abaqus, thus broadening our reach. Hopefully, in the future, open-source software packages such as FEBio or FEniCS will provide 1D truss elements in their default installations.

While we consider the Texas TriValve 1.0 a success, there are many future challenges awaiting us. That is, there are

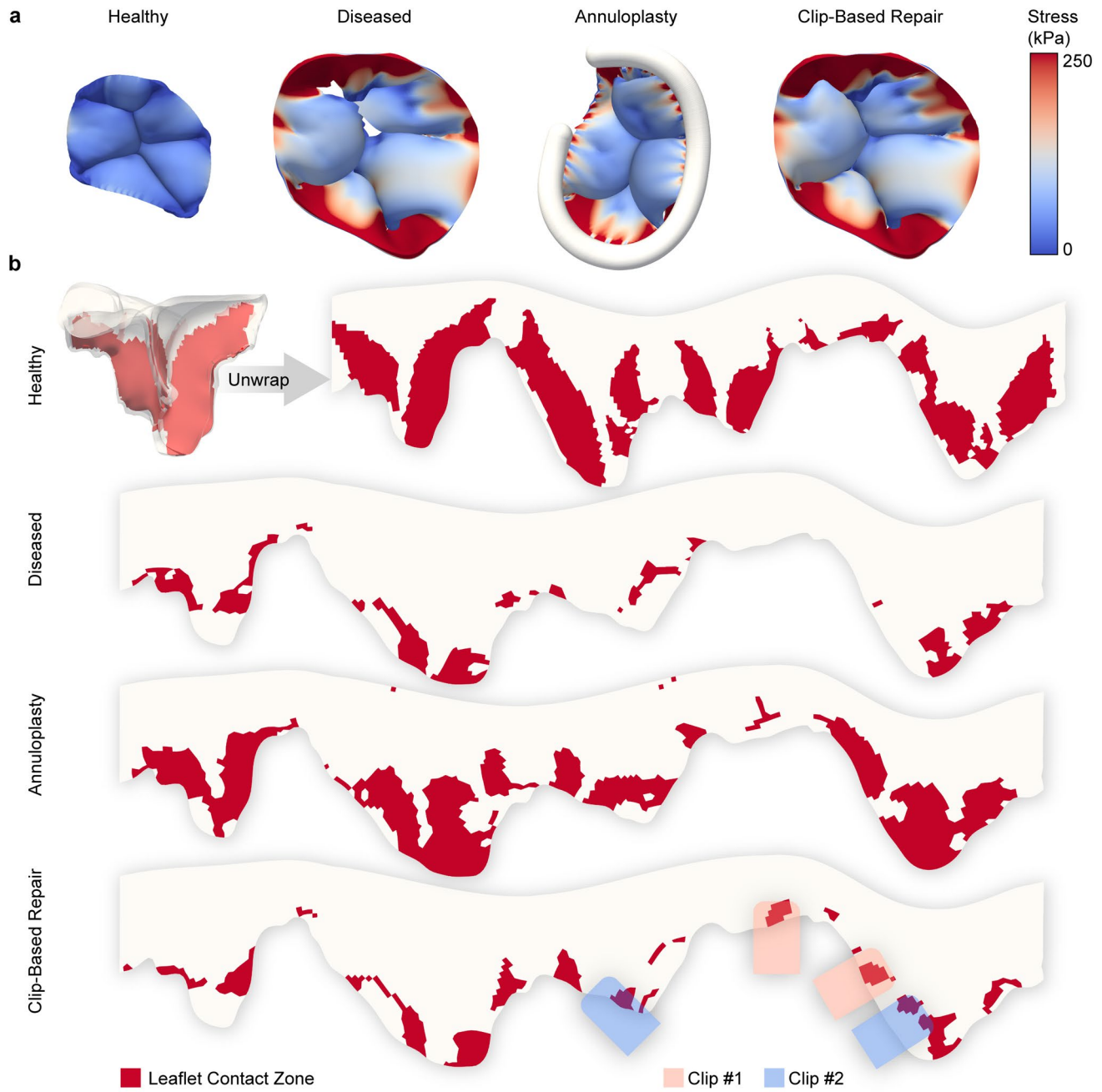

Fig. 7 Outcomes of simulated valve repair strategies: Showcases 1 and 2. **a** Contours of the maximum principal Cauchy stress of the healthy, diseased, and repaired tricuspid valves show that disease (i.e., annular dilation, papillary muscle displacement, and hypertension) induces significant leaflet stress near the annulus and that neither repair technique fundamentally resolves those stresses. **b** Leaflet coaptation areas (in red) projected onto 2D representation of each valve model at end-diastole (white) show that disease significantly lowers the total coaptation area leading to leakage. While annuloplasty restores the coaptation area, clip-based repair does not

limitations to overcome for future generations of this and similar models. For example, this first model uses homogenized material properties across each leaflet and average leaflet thicknesses across the entire tricuspid valve. In future models, we will incorporate spatial heterogeneity in both leaflet thicknesses [27] as well as mechanical properties [56]. Additionally, we do not incorporate the maladaptive effects of functional tricuspid regurgitation, i.e., increased leaflet thickness and stiffness, in our diseased valve model [25]. Furthermore, in this first implementation, we only simulate the elastodynamics of the valve and neglect any effects due to hemodynamic shear despite heart valves' dynamics being inherently a fluid–structure interaction problem [57]. The consequences of this simplification are likely most

impactful on the results of our dynamic simulations. That is, the absence of fluid–structure interaction likely affects the exact timing and magnitude of kinematic and kinetic quantities throughout the cardiac cycle. Future implementations of this and similar models will therefore include blood flow. Also, in the absence of 3D echocardiographic data for the ex vivo beating heart, we are only able to validate our model in 2D. Even worse, because of the echogenicity of our epicardial sonomicrometry markers, we were limited to a single imaging plane. In future studies, we will build valve models directly from 3D echocardiographic images, thereby permitting us to perform 3D spatial comparisons between our simulations and experimental patient data [58]. Thereby, we will also be able to optimize chordal length more confidently than through our current, manual approach [39]. Finally, subject-specificity is important to overcoming the limitations of generic models that miss critical, subject-specific details. For example, generic models always assume that the tricuspid valve has three leaflets. Interestingly, that is only true for 54% of tricuspid valves [59]. Ignoring such subject-specific morphological details in analyses and designs may be, at least in part, responsible for high failure rates of current tricuspid valve repair technologies [60]. However, specificity comes at the cost of poor predictability of general trends. That is, our model is likely inappropriate to study and predict the impact of medical devices on three- or five-leaflet valves. The only path to overcoming the limitation of subject-specificity is to build enough models that sufficiently represent the general population, which we are planning to do.

In conclusion, we (reverse) engineered a high-fidelity model of the human tricuspid valve. The valve is fully subject-specific by accounting for the geometry, material properties, and boundary conditions of a healthy, human tricuspid valve. Through this model, we overcome the limitations of existing computational models that lack subject-specificity. We also validated this model against our own echocardiographic measurements in the beating human heart and compared the simulated kinematics and kinetics of the valve against our own findings and those by others. Additionally, we demonstrated the usefulness of our model by first creating a diseased valve model and then simulating and comparing a surgical and a non-surgical valve repair strategy. Most critically, we make this model openly available for non-commercial use. Thereby, others can use our model toward understanding the healthy, diseased, and repaired tricuspid valve and overcoming our current knowledge gaps about one of our four heart valves. Importantly, we envision this predictive model to be the first in a series of tricuspid valve simulation tools that we will make available to the research community.

Supplementary Information The online version contains supplementary material available at https://doi.org/10.1007/s00366-022-01659-w.

Acknowledgements This research was supported by funding from the American Heart Association via award numbers 18CDA34120028 and 902502, and by the National Heart, Lung, and Blood Institute of the National Institutes of Health via award numbers 1R21HL161832-01 and F31HL145976. The authors would like to thank the Living Heart Team at Abaqus for their technical support and their courtesy software license. We would also like to thank the Texas Advanced Computing Center for the use of their computing resources.

Author contributions MKR and TAT conceived the experiments; MMal., TJ, and WDM conducted the experiments; MMat. performed the simulations and analysed the results. All authors reviewed the manuscript.

Data availability The Abaqus input files that contain all model information and augmented reality files of model results are available through GitHub: https://github.com/SoftTissueBiomechanicsLab/Texas_TriValve.git

Declarations

Conflict of interest Dr. Manuel. K. Rausch has a speaking agreement with Edwards Lifesciences (Irvine, CA). None of the other authors have any potential conflicts of interest.

References

1. Nkomo VT, Gardin JM, Skelton TN, Gottdiener JS, Scott CG, Enriquez-Sarano M (2006) Burden of valvular heart diseases: a population-based study. Lancet 368(9540):1005–1011. https://doi.org/10.1016/S0140-6736(06)69208-8
2. Otto CM, Prendergast B (2014) Aortic-valve stenosis—from patients at risk to severe valve obstruction. N Engl J Med 371(8):744–756. https://doi.org/10.1056/nejmra1313875
3. Dziadzko V, Clavel MA, Dziadzko M, Medina-Inojosa JR, Michelena H, Maalouf J, Nkomo V, Thapa P, Enriquez-Sarano M (2018) Outcome and undertreatment of mitral regurgitation: a community cohort study. The Lancet 391(10124):960–969. https://doi.org/10.1016/S0140-6736(18)30473-2
4. Asmarats L, Taramasso M, Rodés-Cabau J (2019) Tricuspid valve disease: diagnosis, prognosis and management of a rapidly evolving field. Nat Rev Cardiol 16(9):538–554. https://doi.org/10.1038/s41569-019-0186-1
5. Nath J, Foster E, Heidenreich PA (2004) Impact of tricuspid regurgitation on long-term survival. J Am Coll Cardiol 43(3):405–409. https://doi.org/10.1016/j.jacc.2003.09.036
6. Dreyfus GD, Martin RP, Chan KMJ, Dulguerov F, Alexandrescu C (2015) Functional tricuspid regurgitation: a need to revise our understanding. J Am Coll Cardiol 65(21):2331–2336. https://doi.org/10.1016/j.jacc.2015.04.011
7. Rodés-Cabau J, Taramasso M, O'Gara PT (2016) Diagnosis and treatment of tricuspid valve disease: current and future perspectives. The Lancet 388(10058):2431–2442. https://doi.org/10.1016/S0140-6736(16)00740-6
8. Navia JL, Nowicki ER, Blackstone EH, Brozzi NA, Nento DE, Atik FA, Rajeswaran J, Gillinov AM, Svensson LG, Lytle BW (2010) Surgical management of secondary tricuspid valve regurgitation: annulus, commissure, or leaflet procedure? J Thorac

Cardiovasc Surg 139(6):1473–14825. https://doi.org/10.1016/j.jtcvs.2010.02.046
9. Taramasso M, Vanermen H, Maisano F, Guidotti A, La Canna G, Alfieri O (2012) The growing clinical importance of secondary tricuspid regurgitation. J Am Coll Cardiol 59(8):703–710. https://doi.org/10.1016/j.jacc.2011.09.069
10. Algarni KD, Alfonso J, Pragliola C, Kheirallah H, Adam AI, Arafat AA (2021) Long-term outcomes of tricuspid valve repair: the influence of the annuloplasty prosthesis. Ann Thorac Surg 112(5):1493–1500. https://doi.org/10.1016/j.athoracsur.2020.09.038
11. Mas PT, Rodríguez-Palomares JF, Antunes MJ (2015) Secondary tricuspid valve regurgitation: a forgotten entity. Heart 101(22):1840–1848. https://doi.org/10.1136/heartjnl-2014-307252
12. Prihadi EA (2018) Tricuspid valve regurgitation: no longer the "forgotten valve". ESC E-J Cardiol Pract 16
13. Kunzelman KS, Quick DW, Cochran RP (1998) Altered collagen concentration in mitral valve leaflets: Biochemical and finite element analysis. Ann Thorac Surg. https://doi.org/10.1016/S0003-4975(98)01106-0
14. Mesnier J, Alperi A, Panagides V, Bédard E, Salaun E, Philippon F, Rodés-Cabau J (2021) Transcatheter tricuspid valve interventions: current devices and associated evidence. Prog Cardiovasc Dis 69:89–100. https://doi.org/10.1016/j.pcad.2021.11.007
15. Rausch MK, Zöllner AM, Genet M, Baillargeon B, Bothe W, Kuhl E (2017) A virtual sizing tool for mitral valve annuloplasty. Int J Numer Methods Biomed Eng 33(2):53. https://doi.org/10.1002/cnm.2788
16. Stevanella M, Votta E, Lemma M, Antona C, Redaelli A (2010) Finite element modelling of the tricuspid valve: a preliminary study. Med Eng Phys 32(10):1213–1223. https://doi.org/10.1016/j.medengphy.2010.08.013
17. Kong F, Pham T, Martin C, Elefteriades J, McKay R, Primiano C, Sun W (2018) Finite element analysis of annuloplasty and papillary muscle relocation on a patient-specific mitral regurgitation model. PLoS One 13(6):1–15. https://doi.org/10.1371/journal.pone.0198331
18. Kamensky D, Xu F, Lee CH, Yan J, Bazilevs Y, Hsu MC (2018) A contact formulation based on a volumetric potential: Application to isogeometric simulations of atrioventricular valves. Comput Methods Appl Mech Eng 330:522–546. https://doi.org/10.1016/j.cma.2017.11.007
19. Laurence DW, Johnson EL, Hsu MC, Baumwart R, Mir A, Burkhart HM, Holzapfel GA, Wu Y, Lee CH (2020) A pilot in silico modeling-based study of the pathological effects on the biomechanical function of tricuspid valves. Int J Numer Methods Biomed Eng. https://doi.org/10.1002/cnm.3346
20. Singh-Gryzbon S, Sadri V, Toma M, Pierce EL, Wei ZA, Yoganathan AP (2019) Development of a computational method for simulating tricuspid valve dynamics. Ann Biomed Eng. https://doi.org/10.1007/s10439-019-02243-y
21. Laurence DW, Lee CH, Johnson EL, Hsu MC (2021) An in-silico benchmark for the tricuspid heart valve—geometry, finite element mesh, Abaqus simulation, and result data set. Data Brief 39:107664. https://doi.org/10.1016/j.dib.2021.107664
22. Malinowski M, Jazwiec T, Goehler M, Quay N, Bush J, Jovinge S, Rausch MK, Timek TA (2019) Sonomicrometry-derived 3-dimensional geometry of the human tricuspid annulus. J Thorac Cardiovasc Surg 157(4):1452–14611. https://doi.org/10.1016/j.jtcvs.2018.08.110
23. Jensen MO, Siefert AW, Okafor I, Yoganathan AP (2018) In: Sacks MS, Liao J (eds) Measurement technologies for heart valve function. Springer, Cham, pp 115–149, https://doi.org/10.1007/978-3-030-01993-8_6
24. Meador WD, Zhou J, Malinowski M, Jazwiec T, Calve S, Timek TA, Rausch MK (2021) The effects of a simple optical clearing protocol on the mechanics of collagenous soft tissue. J Biomech 122:110413. https://doi.org/10.1016/j.jbiomech.2021.110413
25. Meador WD, Mathur M, Sugerman GP, Malinowski M, Jazwiec T, Wang X, Lacerda CM, Timek TA, Rausch MK (2020) The tricuspid valve also maladapts as shown in sheep with biventricular heart failure. eLife 9:1–22. https://doi.org/10.7554/ELIFE.63855
26. Smith KJ, Mathur M, Meador WD, Phillips-Garcia B, Sugerman GP, Menta AK, Jazwiec T, Malinowski M, Timek TA, Rausch MK (2020) Tricuspid chordae tendineae mechanics: insertion site, leaflet, and size-specific analysis and constitutive modelling. Exp Mech. https://doi.org/10.1007/s11340-020-00594-5
27. Meador WD, Mathur M, Sugerman GP, Jazwiec T, Malinowski M, Bersi MR, Timek TA, Rausch MK (2020) A detailed mechanical and microstructural analysis of ovine tricuspid valve leaflets. Acta Biomater 102:100–113. https://doi.org/10.1016/j.actbio.2019.11.039
28. Pham T, Sulejmani F, Shin E, Wang D, Sun W (2017) Quantification and comparison of the mechanical properties of four human cardiac valves. Acta Biomater 54:345–355. https://doi.org/10.1016/j.actbio.2017.03.026
29. Mathur M, Meador WD, Jazwiec T, Malinowski M, Timek TA, Rausch MK (2020) The effect of downsizing on the normal tricuspid annulus. Ann Biomed Eng 48(2):655–668. https://doi.org/10.1007/s10439-019-02387-x
30. Rausch MK, Malinowski M, Meador WD, Wilton P, Khaghani A, Timek TA (2018) The effect of acute pulmonary hypertension on tricuspid annular height, strain, and curvature in sheep. Cardiovasc Eng Technol 9(3):365–376. https://doi.org/10.1007/s13239-018-0367-9
31. Malinowski M, Schubert H, Wodarek J, Ferguson H, Eberhart L, Langholz D, Jazwiec T, Rausch MK, Timek TA (2018) Tricuspid annular geometry and strain after suture annuloplasty in acute ovine right heart failure. Ann Thorac Surg 106(6):1804–1811. https://doi.org/10.1016/j.athoracsur.2018.05.057
32. Rausch MK, Mathur M, Meador WD (2019) Biomechanics of the tricuspid annulus: a review of the annulus' in vivo dynamics with emphasis on ovine data. GAMM Mitteilungen. https://doi.org/10.1002/gamm.201900012
33. Johnson EL, Laurence DW, Xu F, Crisp CE, Mir A, Burkhart HM, Lee CH, Hsu MC (2021) Parameterization, geometric modeling, and isogeometric analysis of tricuspid valves. Comput Methods Appl Mech Eng. https://doi.org/10.1016/j.cma.2021.113960
34. Silver MD, Lam JH, Ranganathan N, Wigle ED (1971) Morphology of the human tricuspid valve. Circulation 43(3):333–348. https://doi.org/10.1161/01.CIR.43.3.333
35. Khalighi AH, Rego BV, Drach A, Gorman RC, Gorman JH, Sacks MS (2019) Development of a functionally equivalent model of the mitral valve chordae tendineae through topology optimization. Ann Biomed Eng 47(1):60–74. https://doi.org/10.1007/s10439-018-02122-y
36. Drach A, Khalighi AH, Sacks MS (2018) A comprehensive pipeline for multi-resolution modeling of the mitral valve: validation, computational efficiency, and predictive capability. Int J Numer Methods Biomed Eng 34(2):1–30. https://doi.org/10.1002/cnm.2921
37. Wang Q, Sun W (2013) Finite element modeling of mitral valve dynamic deformation using patient-specific multi-slices computed tomography scans. Ann Biomed Eng 41(1):142–153. https://doi.org/10.1007/s10439-012-0620-6
38. Wenk JF, Zhang Z, Cheng G, Malhotra D, Acevedo-Bolton G, Burger M, Suzuki T, Saloner DA, Wallace AW, Guccione JM, Ratcliffe MB (2010) First finite element model of the left ventricle with mitral valve: insights into ischemic mitral regurgitation.

Ann Thorac Surg 89(5):1546–1553. https://doi.org/10.1016/j.athoracsur.2010.02.036
39. Kong F, Pham T, Martin C, McKay R, Primiano C, Hashim S, Kodali S, Sun W (2018) Finite element analysis of tricuspid valve deformation from multi-slice computed tomography images. Ann Biomed Eng 46(8):1112–1127. https://doi.org/10.1007/s10439-018-2024-8
40. Pham T, Kong F, Martin C, Wang Q, Primiano C, McKay R, Elefteriades J, Sun W (2017) Finite element analysis of patient-specific mitral valve with mitral regurgitation. Cardiovasc Eng Technol 8(1):3–16. https://doi.org/10.1007/s13239-016-0291-9
41. Peirlinck M, Costabal FS, Yao J, Guccione JM, Tripathy S, Wang Y, Ozturk D, Segars P, Morrison TM, Levine S, Kuhl E (2021) Precision medicine in human heart modeling: perspectives, challenges, and opportunities. Biomech Model Mechanobiol 20(3):803–831. https://doi.org/10.1007/s10237-021-01421-z
42. Dassault Systemes (SIMULIA), Providence, RI: Section 1.2.9. Abaqus User Subroutine Reference Guide, (2014)
43. Dassault Systemes (SIMULIA), Providence, RI: Section 38.2.3. Abaqus Analysis User's Guide 6.14, (2014)
44. Ring L, Rana BS, Kydd A, Boyd J, Parker K, Rusk RA (2012) Dynamics of the tricuspid valve annulus in normal and dilated right hearts: A three-dimensional transoesophageal echocardiography study. Eur Heart J Cardiovasc Imaging 13(9):756–762. https://doi.org/10.1093/ehjci/jes040
45. Spinner EM, Lerakis S, Higginson J, Pernetz M, Howell S, Veledar E, Yoganathan AP (2011) Correlates of tricuspid regurgitation as determined by 3D echocardiography: pulmonary arterial pressure, ventricle geometry, annular dilatation and papillary muscle displacement. Circ Cardiovasc Imaging Cardiovasc Imaging 5(1):43–50. https://doi.org/10.1161/CIRCIMAGING.111.965707
46. Nickenig G, Kowalski M, Hausleiter J, Braun D, Schofer J, Yzeiraj E, Rudolph V, Friedrichs K, Maisano F, Taramasso M, Fam N, Bianchi G, Bedogni F, Denti P, Alfieri O, Latib A, Colombo A, Hammerstingl C, Schueler R (2017) Transcatheter treatment of severe tricuspid regurgitation with the edge-to-edge mitraclip technique. Circulation 135(19):1802–1814. https://doi.org/10.1161/CIRCULATIONAHA.116.024848
47. Mathur M, Meador WD, Jazwiec T, Malinowski M, Timek TA, Rausch MK (2020) Tricuspid valve annuloplasty alters leaflet mechanics. Ann Biomed Eng. https://doi.org/10.1007/s10439-020-02586-x
48. Lesevic H, Sonne C, Kasel AM, Breuer D, Kastrati A, Schunkert H, Ott I (2017) Implantation of a MitraClip between two previously implanted MitraClips to treat recurrent severe mitral regurgitation. J Cardiol Cases 15(2):50–52. https://doi.org/10.1016/j.jccase.2016.10.009
49. Kong F, Caballero A, McKay R, Sun W (2020) Finite element analysis of MitraClip procedure on a patient-specific model with functional mitral regurgitation. J Biomech 104:109730. https://doi.org/10.1016/j.jbiomech.2020.109730
50. Sturla F, Redaelli A, Puppini G, Onorati F, Faggian G, Votta E (2015) Functional and biomechanical effects of the edge-to-edge repair in the setting of mitral regurgitation: consolidated knowledge and novel tools to gain insight into its percutaneous implementation. Cardiovasc Eng Technol 6(2):117–140. https://doi.org/10.1007/s13239-014-0208-4
51. Biaggi P, Jedrzkiewicz S, Gruner C, Meineri M, Karski J, Vegas A, Tanner FC, Rakowski H, Ivanov J, David TE, Woo A (2012) Quantification of mitral valve anatomy by three-dimensional transesophageal echocardiography in mitral valve prolapse predicts surgical anatomy and the complexity of mitral valve repair. J Am Soc Echocardiogr 25(7):758–765. https://doi.org/10.1016/j.echo.2012.03.010
52. Mathur M, Jazwiec T, Meador WD, Malinowski M, Goehler M, Ferguson H, Timek TA, Rausch MK (2019) Tricuspid valve leaflet strains in the beating ovine heart. Biomech Model Mechanobiol. https://doi.org/10.1007/s10237-019-01148-y
53. Dolensky JR, Casa LDC, Siefert AW, Yoganathan AP (2013) In vitro assessment of available coaptation area as a novel metric for the quantification of tricuspid valve coaptation. J Biomech 46(4):832–836. https://doi.org/10.1016/j.jbiomech.2012.11.054
54. Czapla J, Claus I, Martens T, Philipsen T, Van Belleghem Y, François K, Bove T (2021) Midterm comparison between different annuloplasty techniques for functional tricuspid regurgitation. Ann Thorac Surg. https://doi.org/10.1016/j.athoracsur.2021.07.073
55. Maas SA, LaBelle SA, Ateshian GA, Weiss JA (2018) A plugin framework for extending the simulation capabilities of febio. Biophys J 115(9):1630–1637
56. Laurence D, Ross C, Jett S, Johns C, Echols A, Baumwart R, Towner R, Liao J, Bajona P, Wu Y, Lee CH (2019) An investigation of regional variations in the biaxial mechanical properties and stress relaxation behaviors of porcine atrioventricular heart valve leaflets. J Biomech 83:16–27. https://doi.org/10.1016/j.jbiomech.2018.11.015
57. Luraghi G, Wu W, De Gaetano F, Rodriguez Matas JF, Moggridge GD, Serrani M, Stasiak J, Costantino ML, Migliavacca F (2017) Evaluation of an aortic valve prosthesis: fluid-structure interaction or structural simulation? J Biomech 58:45–51. https://doi.org/10.1016/j.jbiomech.2017.04.004
58. Pouch AM, Aly AH, Lasso A, Nguyen AV, Scanlan AB, McGowan FX, Fichtinger G, Gorman RC, Gorman JH, Yushkevich PA, Jolley MA (2017) Image segmentation and modeling of the pediatric tricuspid valve in hypoplastic left heart syndrome. In: Pop M, Wright GA (eds) Functional imaging and modelling of the heart. Springer, Cham, pp 95–105
59. Hahn RT, Weckbach LT, Noack T, Hamid N, Kitamura M, Bae R, Lurz P, Kodali SK, Sorajja P, Hausleiter J, Nabauer M (2021) Proposal for a standard echocardiographic tricuspid valve nomenclature. JACC Cardiovasc Imaging 14(7):1299–1305. https://doi.org/10.1016/j.jcmg.2021.01.012
60. Sugiura A, Tanaka T, Kavsur R, Öztürk C, Vogelhuber J, Wilde N, Becher MU, Zimmer S, Nickenig G, Weber M (2021) Leaflet configuration and residual tricuspid regurgitation after transcatheter edge-to-edge tricuspid repair. JACC Cardiovasc Interv 14(20):2260–2270. https://doi.org/10.1016/j.jcin.2021.07.048